Tribological Behavior of a Carbon-Nanofiber-Modified Santoprene Thermoplastic Elastomer Under Dry Sliding and Fretting Conditions Against Steel

J. Karger-Kocsis,[1] D. Felhös,[1] R. Thomann[2]

[1]*Institut für Verbundwerkstoffe GmbH, Technical University Kaiserslautern, Erwin-Schrödinger-Straße 58, D-67663, Kaiserslautern, Germany*
[2]*Freiburger Materialforschungszentrum, Albert-Ludwigs-Universität Freiburg, Stefan Meier Straße 31, D-79104 Freiburg, Germany*

Received 21 June 2007; accepted 16 September 2007
DOI 10.1002/app.27429
Published online 11 January 2008 in Wiley InterScience (www.interscience.wiley.com).

ABSTRACT: Vapor-grown carbon nanofiber (CNF) was incorporated in concentrations of 0.9 and 4.5 wt % into a thermoplastic dynamic vulcanizate (TPV), Santoprene 8201-80HT, by melt blending. CNF was introduced from its aqueous dispersion with crumb ethylene/propylene/diene rubber as the carrier. The dispersion of the CNF was studied with transmission electron microscopy. The TPV compounds were characterized by dynamic mechanical thermal analysis, hardness measurements, and tensile and tear tests. For their tribotesting, different test configurations (pin on plate and roller on plate, where the plate was always the rubber) were adopted. The oscillation wear (fretting) of the CNF-modified TPVs was also studied. The coefficient of friction and specific wear rate of the TPVs were determined for each tribotest. These friction and wear parameters strongly depended on the tribotests' configurations. With increasing CNF content, the coefficient of friction and wear rate decreased for the pin-on-plate configuration. On the other hand, no such clear tendency could be deduced for the roller-on-plate configuration and fretting. The worn surfaces of the specimens were inspected with scanning electron microscopy, and the related mechanisms were discussed. © 2008 Wiley Periodicals, Inc. J Appl Polym Sci 108: 724–730, 2008

Key words: nanotechnology; poly(propylene) (PP); rubber; structure-property relations; thermoplastics

INTRODUCTION

Vapor-grown carbon nanofibers (CNFs) can be produced continuously in a single step by thermal decomposition of hydrocarbons (>1000°C) in the presence of suitable metallic catalysis. This results in an advantageous performance/price ratio, making CNFs attractive property modifiers for polymers, including rubbers. CNFs possess a small diameter (<100 nm) and a very high aspect ratio (>200) with a rather high graphitization degree (≈70%) and specific surface area (>100 m^2/g). As a result, CNFs are being explored as potential reinforcements and electrically conductive fillers.[1] The driving force of the related research and development activity is the high aspect ratio of CNF.[1,2] However, the advantageous high aspect ratio can hardly be exploited as CNFs are entangled and held tightly together by van der Waals forces. To support the disentanglement, the usual strategy is the functionalization of CNF (to trigger the interaction with the polymer matrix) and/or the application of high shear/elongational stresses during the composite production (e.g., melt blending and fiber spinning; see refs. 1–4 and references therein). Based on the finding that carbon nanotubes can be well dispersed (exfoliated) in aqueous media (e.g., ref. 5), the related knowledge has been transferred to the preparation of rubber nanocomposites through the use of the latex compounding route (e.g., ref. 6). As emphasized previously, a substantial amount of work on CNFs has already addressed improvements in the mechanical and electrical properties. In contrast, only a few publications have been devoted to tribological aspects of CNF-modified polymers,[7,8] although CNF seems to be a promising additive to reduce friction and enhance the resistance to wear. It is intuitive that apart from its reinforcing effect, CNF may work as a solid-phase lubricant in polymers. The resistance to wear of polytetrafluoroethylene was increased by more than 1 order of magnitude with less than 3 wt % CNF under dry sliding conditions.[8] On the other hand, a markedly smaller improvement was noticed for ultrahigh-molecular-weight polyethylene when modi-

Correspondence to: J. Karger-Kocsis (karger@ivw.uni-kl.de).
Contract grant sponsor: Knowledge-based radical innovation surfacing for tribology and advance lubrication (KRISTAL) (integrated project of the European Union); contract grant number: NMP3-CT-2005-515837.

Journal of Applied Polymer Science, Vol. 108, 724–730 (2008)

fied with 5 or 10 wt % CNF. The CNF in the cited study was predispersed in paraffinic oil before its introduction into the ultrahigh-molecular-weight polyethylene during extrusion melt compounding.[7]

Surprisingly, no report is available on the tribological behavior of carbon-nanotube-reinforced and CNF-reinforced thermoset and thermoplastic rubbers.[9] It is usually assumed that these novel fillers may replace traditional ones (carbon black or silica) when incorporated even in lesser amounts. It is noteworthy that the sliding wear performance of thermoplastic elastomers, produced by dynamic vulcanization (described, for example, in ref. 10), has not yet been studied. This is at odds with the widespread use of such thermoplastic dynamic vulcanizates (TPVs) in products for which the resistance to sliding wear is crucial (windshield wipers, glass window seals in cars, etc.). On the other hand, some useful information on the scratch resistance of TPVs, which is of paramount importance for automotive inner parts, is already available.[11]

The purpose of this work was to study the mechanical and dry sliding properties of CNF-modified TPV systems. To get deeper insight into the friction and wear of the related nanocomposites, various tribotests were used. All tribological tests were run against steel under dry (unlubricated) conditions.

EXPERIMENTAL

Materials and specimen preparation

TPV (Santoprene 8201-80HT) was procured from Advanced Elastomer Systems (Akron, OH). This TPV grade contained, in addition to the usual components [polypropylene (PP) as a continuous phase, crosslinked ethylene/propylene/diene rubber (EPDM) as a dispersed phase, and oil as a processing aid], some polyethylene. The latter may be derived from a poly(propylene-*block*-ethylene) copolymer, used as a matrix in this case, in which the crosslinked submicrometer-sized EPDM particles are dispersed.[12] An aqueous dispersion of CNF with a concentration of 15 g/L was donated by Grupo Antolin (Burgos, Spain). The related CNF had a diameter range of 20–80 nm, a graphitization degree of about 70 wt %, and a metallic particle content of 6–8 wt %. Although the length of the CNFs from Grupo Antolin is usually greater than 30 μm, no information was available on the aspect ratio of the CNF in the aqueous dispersion delivered. To get a good CNF dispersion in the TPV, crumb EPDM rubber with a high ethylene content (71 wt %) was used as a carrier (Buna AP447, Bayer, Leverkusen, Germany). On the porous EPDM crumbs, the CNF dispersion was sprayed (in the required amount), and then the water was evaporated. The dried EPDM/CNF composition was introduced into the TPV via melt mixing in a Brabender (Duisburg, Germany) plasticoder. The temperature of the kneading chamber (55 cm^3) was set at 200°C, and the mixing lasted for 6 min at 60 rpm with the kneaders. The composition of the TPV compound was as follows: TPV, 95 parts; EPDM, 5 parts; and CNF, 0, 1, or 5 parts. The compounds taken from the Brabender chamber were pressed into approximately 2-mm-thick sheets by hot pressing at 200°C.

Dispersion of the CNF

Information about the dispersion and aspect ratio of the CNF was received from transmission electron microscopy (TEM) investigations. The TEM measurement were carried out with a Zeiss (Oberkochen, Germany) Leo 912 Omega transmission electron microscope with an acceleration voltage of 120 kV. The specimens were prepared with a Leica Ultracut UCT ultramicrotome equipped with a cryochamber (Vienna, Austria). Thin sections of about 50 nm were cut with a Diatome diamond knife (Hatfield, PA, USA) at −120°C. Some sections were stained by exposure to gaseous OsO_4.

Mechanical tests

Dynamic mechanical thermal analysis (DMTA)

DMTA spectra were recorded on rectangular specimens (length × width × thickness = 20 × 10 × ~ 2 mm^3) in a tension mode as a function of temperature (from −100 to +100°C) and at a frequency of 10 Hz with a Q800 device from TA Instruments (New Castle, DE). Tests were run at a constant strain (0.01%) through the heating of the specimens in a stepwise manner (stepping by 5°C followed by an equilibration time of 3 min at each temperature).

Hardness and density

The Shore A hardness of the rubbers was determined according to ISO 868 with a hardness measuring device from Zwick (Ulm, Germany). The universal hardness was determined by the DIN 50359-1 standard with a Shimadzu DUH 202 device with a Vickers-type diamond indenter. During the microhardness measurements, the maximal load was 5 mN, and the holding time at the maximal loading (i.e., prior downloading) was 2 s. For the density determination, the Archimedes principle (buoyancy method with water) was adopted according to ISO 1183. The density measurement kit was adjusted to a Mettler (Giessen, Germany) AT261 microbalance.

Mechanical properties

Tensile tests were carried out on 2-mm-thick dumbbells (type S1 according to DIN 53504) on a Zwick 1445 universal testing machine at a deformation rate of 500 mm/min. From the related stress–strain curves, apart from the ultimate properties, the stress values at 100 and 200% elongations, termed M-100 and M-200, respectively, were also read (ISO 37). The tear strength was determined on angle-type specimens cut at a 500 mm/min deformation rate (ISO 34-1 standard). All mechanical tests were performed at the ambient temperature with a minimum of five specimens.

Wear tests

Sliding friction and wear tests

Friction and wear characteristics were determined in a pin-on-plate (POP) configuration (the pin was steel, and the plate was rubber) with a Wazau (Berlin, Germany) device in which a steel pin (100Cr6; arithmetical roughness $\approx$ 1 μm) with a hemispherical tip 10 mm in diameter rotated along a circular path (diameter = 33 mm). The pin was pushed against the rubber plate with a given load. The following parameters were selected for this configuration: normal load, 2 N; sliding speed, 250 mm/s; and duration, 1.5 h. Through the measurement of both the normal and friction force components via a torque load cell, the coefficient of friction (COF) values were calculated and monitored during the test.

To study the sliding wear, a further test, termed roller on plate (ROP; the roller was steel, and the plate was rubber), was also used. A rotating steel roller (100Cr6, diameter = 10 mm, width = 20 mm, arithmetical roughness $\approx$ 0.9 μm) was pressed against a rubber strip 9 mm wide in an SOP 3000 tribotester (Dr Tillwich GmbH, Horb-Ahldorf, Germany). The frictional force induced by the torque was measured online, and thus the COF was registered during the test. The test parameters were as follows: load, 4 N; sliding speed, 250 mm/s; and duration, maximum 1.5 h.

The third tribotester was a fretting machine (SRV III, Optimol, Munich, Germany) in which a cylinder was oscillating on the surface of the fixed rubber specimen when they were pressed against each other with a given load. The diameter and contact length of the steel cylinder (arithmetical roughness $\approx$ 0.9 μm) were 15 and 12 mm, respectively. The applied normal load was 10 N, the frequency of the oscillation was 10 Hz, the stroke was 2 mm, and the duration of the measurements was 3 h.

The test configurations are depicted schematically in Figure 1. The testing parameters along with basic characteristics of the testing rigs are listed in Table I. Wear parameters were deduced from three parallel tests.

The specific wear rate (W_s) was determined as follows:

$$W_s = \frac{\Delta m}{\rho \times F \times L} \quad (1)$$

where Δm is the mass loss recorded gravimetrically, ρ is the density, F is the normal force, and L is the overall sliding distance.

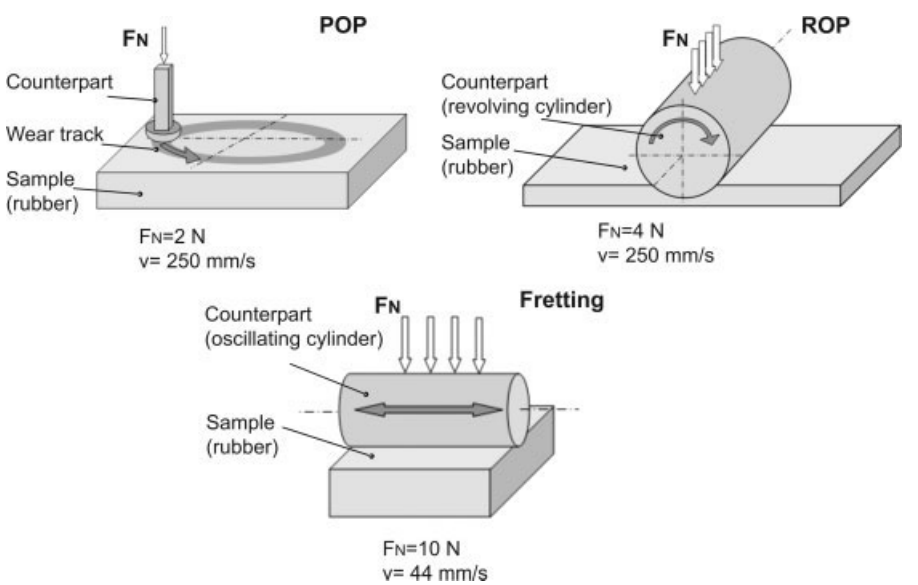

Figure 1 Schematic setup of the tribotesting devices used. Fretting indicates an oscillating steel cylinder on a rubber plate.

TABLE I
Test Parameters and Basic Characteristics of the Tribotests

Test parameter	POP	ROP	Fretting
Diameter of the counterpart (mm)	10	10	15
Contact length (mm)	—	8.5	12
Normal load (N)	2	4	10
Revolution number/frequency (rpm/Hz)	144	137	10
Radius/amplitude of the motion (mm)	16.5	—	2
Arithmetical roughness of the counterpart (μm)	1	0.9	0.9
Average sliding speed (mm/s)	248	251	44
Overall sliding distance (m)	1343	1357	432

Wear mechanisms

The worn surfaces of the specimens were inspected with a scanning electron microscope (JSM5400, JEOL, Tokyo, Japan). Before the scanning electron microscopy (SEM) investigation, the specimens were sputtered with an Au/Pd alloy with a device from Balzers (Liechtenstein).

RESULTS AND DISCUSSION

CNF dispersion

Figure 2(a) shows that the CNF was highly fragmented. Therefore, it is supposed that the dispersion of CNF was produced by ball milling. The diameter of the CNF is less than 100 nm, being in line with the producer's information. On the other hand, the length of the CNF is less than 1 μm, resulting in an aspect ratio of less than 10. The TEM picture of a stained specimen allows us to locate the CNFs. The PP phase has a cloudy structure in Figure 2(b) because of its crystalline nature, whereas the crosslinked EPDM particles (in the submicrometer range) of the initial TPV appear white. The matrix is given by the PP. The CNF is preferentially embedded in the PP. A possible explanation for this finding is the compatibility between the polyethylene phase of the PP block copolymer in the initial TPV and the ethylene-rich (and thus semicrystalline) uncrosslinked EPDM, which is used as a carrier for the CNF in this work.

TPV characteristics

The slight reinforcing effect of the CNF is reflected by the monotonous small decrease in the mechanical loss peak (tan δ) with an increasing amount of CNF. The glass-transition temperature ($T_g = -55°C$) was not influenced by the amount of the CNF. According to the rubber elasticity theory, the inverse of the plateau modulus ($1/E_{pl}$) at a given temperature above T_g correlates with the mean molecular mass between crosslinks (M_c):

$$E_{pl} = \frac{3 \times \rho \times RT}{M_c} \tag{2}$$

where E_{pl} is the modulus at 273 K, R is the universal gas constant [8.314 J/(K mol)], and T is the absolute temperature (i.e., 273 K).

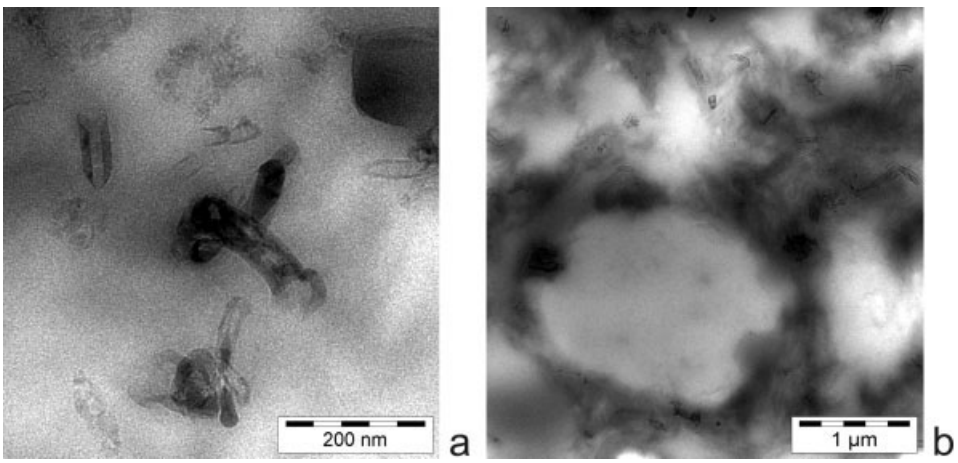

Figure 2 TEM pictures showing (a) the size (without staining) and (b) the dispersion (after staining with OsO_4) of CNF in the TPV/EPDM/CNF compound (100/5/1 by parts).

TABLE II
Network-Related and Mechanical Data for the TPV Rubbers with and Without CNF Fillers

	95/5 TPV/ EPDM	95/5/1 TPV/ EPDM/CNF	95/5/5 TPV/ EPDM/CNF
M_c (g/mol)	67	56	55
ν_c ($10^{+26} \times m^{-3}$)	87	103	106
Tan δ at T_g	0.267	0.260	0.254
Density (g/cm^3)	0.945	0.950	0.963
Shore A (°)	73.5	74	77
Universal hardness (MPa)	18.1	24.5	22.3
M-100 (MPa)	3.2	3.6	3.6
M-200 (MPa)	4	4.5	4.6
Tensile strength (MPa)	6.6	6.5	4.8
Tensile strain (%)	496	427	240
Tear strength (kN/m)	27.5	27.4	27.8

[a] The data were taken from ref. 1.

Alternatively, the apparent crosslink density (ν_c) can be considered:

$$\upsilon_c = \frac{N \times \rho}{M_c} \quad (3)$$

where N is the Avogadro or Loschmidt number (6.023×10^{23} mol^{-1}).

It has to be emphasized that both M_c and ν_c are apparent values. The network-related data are summarized in Table II.

With an increasing amount of CNF, one can observe a slight increase in the Shore A hardness and universal hardness and in the M-100 and M-200 moduli as well. The ultimate tensile strength and strain values decreased with increasing CNF content in the TPVs. This is in concert with the TEM results showing that the CNF is located in the matrix phase of the TPV. The tear strength did not change with the CNF content in the TPV (cf. Table II).

Comparison of the tribotesting conditions

The average sliding speeds of the steel counterparts compared to the fixed rubber specimens are the same for the POP and ROP tests, whereas the value is markedly smaller for the fretting test (cf. Table I). During the POP and ROP tests, pure sliding appears between the steel counterpart and the rubber specimen. Although the relative sliding speed may change across the contact area, the sliding direction remains the same in every moment. During fretting, the direction of the relative displacement is reciprocating between the surfaces of the rubber and the steel cylinder. The maximum and average contact pressure data, calculated by the Hertzian theory are summarized in Table III.

COF

Figure 3 presents the effects of the CNF on the COF of the TPVs. One can recognize that the change in the COF strongly depends on the configuration of the related tribotests. In POP, the COF slightly decreases with increasing CNF content. On the other hand, the opposite tendency holds for ROP and fretting.

Specific wear rate

Considering the specific wear rate results, we can see that their differences may cover some orders of magnitude (cf. Fig. 4). The most severe wear is caused by the POP tests. The incorporation of CNF slightly reduces the specific wear rate of the corresponding TPV in POP. Testing the TPVs in the ROP

TABLE III
Maximum and Average Contact Pressure Data According to the Hertzian Theory for the Different Test Rigs and TPVs

		Santoprene 8201-80HT + 5 phr AP447	Santoprene 8201-80HT + 5 phr AP447 + 1 phr CNF	Santoprene 8201-80HT + 5 phr AP447 + 5 phr CNF
Maximum contact pressure (running in; MPa)	POP	4.67	5.25	5.43
	ROP	1.56	1.70	1.75
	Fretting	1.69	1.85	1.89
Average contact pressure (running in; MPa)	POP	3.12	3.5	3.62
	ROP	1.23	1.34	1.37
	Fretting	1.33	1.45	1.49

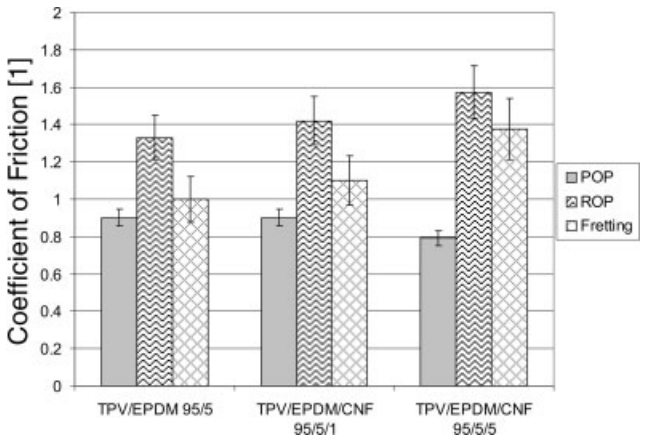

Figure 3 Measured COF values (steady state) in the POP, ROP, and fretting tests.

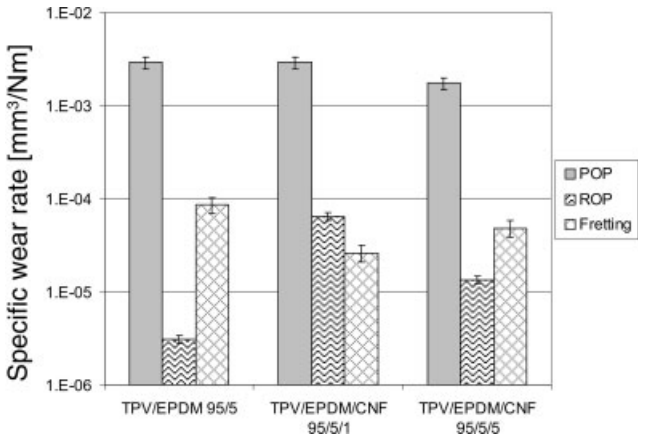

Figure 4 Specific wear rate data for the POP, ROP, and fretting tests.

device, we found a very low specific wear rate for the initial TPV. This excellent wear resistance deteriorated with the addition of 1 phr CNF, but further incorporation of CNF (5 phr) improved again the tribological performance. Nevertheless, the specific wear rate of the unfilled TPV was not reached.

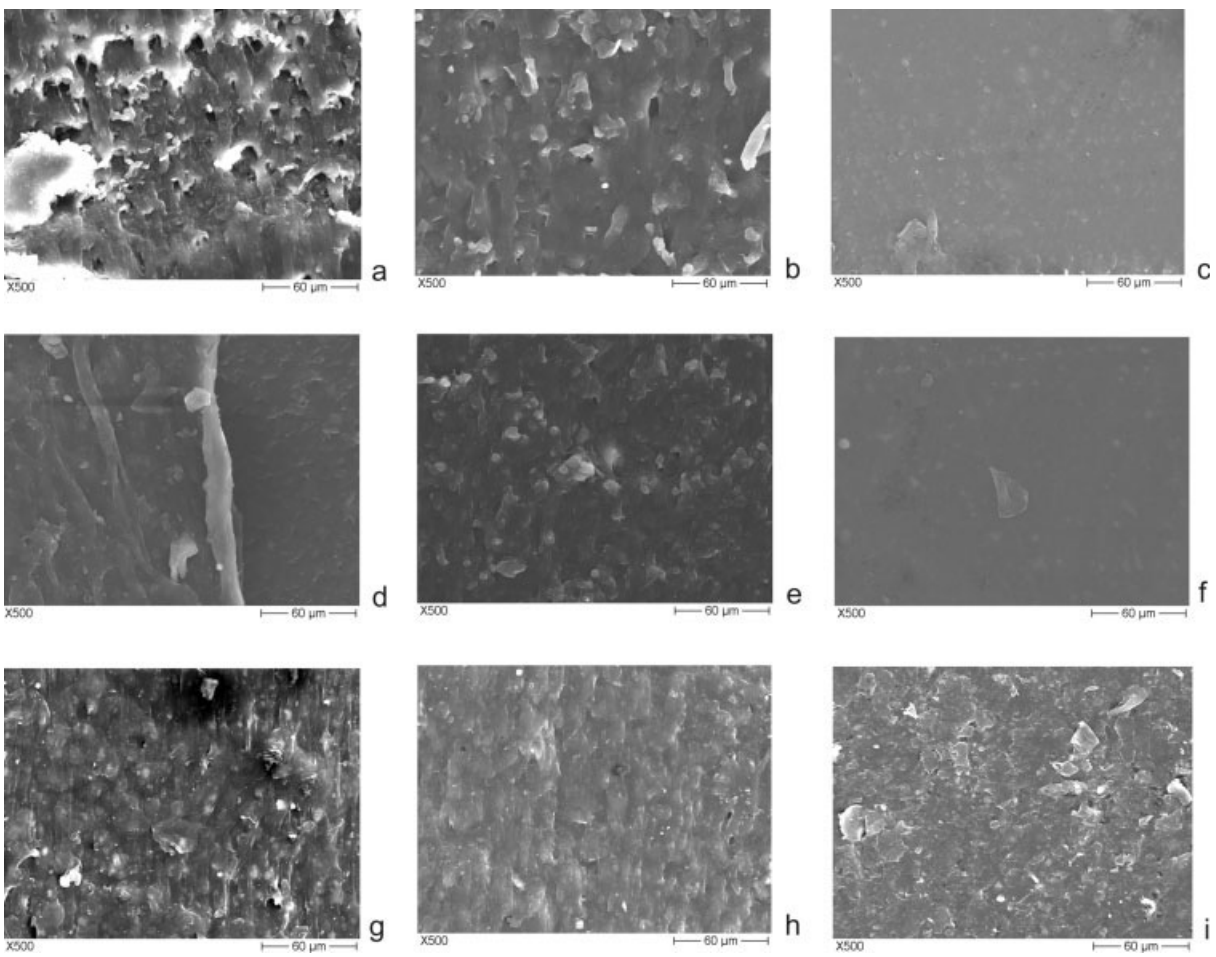

Figure 5 SEM pictures taken from the worn surfaces of TPV/EPDM (95/5 by parts; upper row), TPV/EPDM/CNF (95/5/1 by parts; middle row), and TPV/EPDM/CNF (95/5/5 by parts; bottom row) after (a,d,g) POP, (b,e,h) ROP, and (c,f,i) fretting tests. The sliding and oscillation directions were downward.

The wear resistance to fretting was improved by CNF filling, especially at its low loading (1 phr; cf. Fig. 4).

Wear mechanisms

Characteristic SEM pictures taken from the worn tracks of the TPV stocks after the various tribotests are presented in Figure 5.

POP tests

The worn surface of the parent TPV/EPDM (95/5) stock shows some peculiar features. Although one can see large debris on the surface, which is ironed in the direction of the sliding, the wear mechanism is tongue formation with extensive chipping [cf. Fig. 5(a)]. When 1 phr CNF is incorporated into the TPV matrix, the wear track becomes smoother after the POP test. However, tongues along with roll debris are discernible [cf. Fig. 5(d)]. With increasing CNF content, one can again resolve tongues, which are partly molten and oriented in the sliding direction. On the other hand, the chip formation is markedly reduced compared to that of the parent compound [cf. Fig. 5(a,g)].

ROP tests

After the ROP test in the worn surface of the parent compound (i.e., TPV/EPDM = 95/5 parts), one can see large particles that were chipped off or formed by rolling [cf. Fig. 5(b)]. In the presence of 1 phr CNF filler, the chipping is reduced, and the tongues seem to be less prone to break off [cf. Fig. 5(e)]. With 5 phr CNF, a smeared (ironed) surface can be found without very worn particles [cf. Fig. 5(h)].

Fretting test

The SEM pictures taken from the worn surfaces of the parent and 1 phr CNF containing TPV compounds are very similar to each other. The related surfaces are smooth and rarely show some tongues [cf. Figs. 5(c,f)]. With 5 phr CNF, the surface becomes cracked, and debris appears in the wear track [cf. Fig. 5(i)].

The aforementioned wear mechanisms are basically in line with the COF and specific wear data (cf. Figs. 3 and 4). Deviations can be attributed to the interplay of the following effects caused by the incorporated CNF and EPDM: morphology and/or crystallinity changes and selective oil absorption.

CONCLUSIONS

This work was devoted to studying the effects of CNF on the dry sliding behavior of TPVs in various test configurations. Crumb EPDM of a high ethylene content was spray-coated with an aqueous dispersion of the CNF, which was then dried and melt-blended with the TPV (Santoprene grade). The CNF content was 1 or 5 phr (corresponding to 0.9 and 4.5 wt %). On the basis of this work, the following conclusions can be drawn:

- The CNF was preferentially located in the phase PP–EPDM carrier. CNF was not present in the crosslinked EPDM particles of the parent TPV.
- Both the COF and the specific wear rate data strongly depended on the tribotest configurations. The COF was reduced with increasing CNF content for POP, whereas an opposite trend was deduced for ROP and fretting tests. The specific wear rate was slightly reduced in the presence of CNF in POP and fretting, whereas it was markedly enhanced in ROP measurements.

The authors thank G. Mencia and N. Marinova (Institut für Verbundwerkstoffe (IVW), Kaiserslautern, Germany) for their involvement in the fretting and POP and ROP tests, respectively.

References

1. Tibbets, G. G.; Lake, M. L.; Strong, K. L.; Rice, B. P. Compos Sci Technol 2007, 67, 1709.
2. Hammel, E.; Tang, X.; Trampert, M.; Schmitt, T.; Mauthner, K.; Eder, A.; Pötschke, P. Carbon 2004, 42, 1153.
3. Kelarakis, A.; Yoon, K.; Sics, I.; Somani, R. H.; Hsiao, B. S.; Chu, B. Polymer 2005, 46, 5103.
4. Hasan, M. M.; Zhou, Y.; Jeelani, S. Mater Lett 2007, 61, 1134.
5. Loos, J.; Alexeev, A.; Grossiord, N.; Koning, C. E.; Regev, O. Ultramicroscopy 2005, 104, 160.
6. Wang, J. D.; Zhu, Y. F.; Zhou, X. W.; Sui, G.; Liang, J. J Appl Polym Sci 2006, 100, 4697.
7. Galetz, M. C.; Blaß, T.; Ruckdäschel, H.; Sandler, J. K. W.; Altstädt, V.; Glatzel, U. J Appl Polym Sci 2007, 104, 4173.
8. Shi, Y.; Feng, X.; Wang, H.; Lu, X.; Shen, J. J Appl Polym Sci 2007, 104, 2430.
9. Karger-Kocsis, J.; Felhös, D. In Tribology of Polymeric Nanocomposites; Friedrich, K.; Schlarb, A. K., Eds.; Elsevier: Amsterdam, 2008 (in press).
10. Karger-Kocsis, J. In Polymer Blends and Alloys; Shonaike, G. O.; Simon, G. P., Eds.; Marcel Dekker: New York, 1999; Chapter 5, p 125.
11. Brostow, W.; Lobland, H. E. H.; Narkis, M. J Mater Res 2006, 21, 2422.
12. Karger-Kocsis, J.; Felhös, D.; Xu, D.; Schlarb, A. K. Wear, (2007). doi: 10.1016/j.wear.2007.10.010.